Int J Adv Manuf Technol (2017) 88:3429–3436
DOI 10.1007/s00170-016-9047-9

ORIGINAL ARTICLE

Phenomenological modelling of micro-cutting based on experimental results

Romain Piquard[1,2] · **Sébastien Thibaud**[1] · **Alain D'Acunto**[2] · **Michaël Fontaine**[1] · **Daniel Dudzinski**[2]

Received: 15 July 2015 / Accepted: 13 June 2016 / Published online: 21 June 2016

Abstract In micro-milling, cutting forces are driven by many parameters, including feed per tooth, depth of cut, rake angle and machined material. Because of size effects, issues inherent in the micro-milling process, such as chatter, edge radius or tool deflection, influence the cutting forces making it difficult to understand the process. To overcome this problem, the best solution is to perform experiments independently on each parameter. With orthogonal and oblique micro-cutting experiments, chip formation is investigated with fewer parameters. This study aimed to model micro-cutting using the results obtained from orthogonal and oblique micro-cutting experiments, based on tube turning ignoring dynamic considerations. It was experimentally observed that a jump in cutting forces occurs when the uncut chip thickness decreases, described as a transient regime between ploughing and shearing dominant regimes. The ploughing regime for low uncut chip thicknesses is characterised by a normal force greater than the cutting force. At higher uncut chip thicknesses, the cutting force is dominant. A phenomenological model was developed to take into account the divergence in cutting forces at low uncut chip thicknesses. The model was divided into two terms that model, respectively, ploughing and shearing regimes with a continuous transient regime. The model reproduced the behaviour quite well and could be enriched with more parameters.

Keywords Micro-cutting · Cutting forces · Modelling · Elementary cutting · Ploughing

✉ Romain Piquard
romain.piquard@femto-st.fr

[1] Department of Applied Mechanics, FEMTO-ST Institute, UMR 6174, UBFC/UFC/ENSMM/UTBM/CNRS, 24 rue de l'Epitaphe, 25000 Besançon, France

[2] LEM3, UMR 7239, Université de Lorraine/Arts et Métiers ParisTech/ENIM/CNRS, 4 rue Augustin Fresnel, 57078 Metz, France

Notations

h	Uncut chip thickness (μm)
w	Cutting width (μm)
r_β	Cutting edge radius (μm)
γ	Rake angle (°)
λ_s,	Inclination angle (°) (along cut surface normal)
V_c	Cutting speed (m/min)
F_x	Measured force along dynamometer's X axis (N)
F_y	Measured force along dynamometer's Y axis (N)
F_x	Measured force along dynamometer's Z axis (N)
F_c	Cutting force along cutting speed direction (N)
F_f	Cutting force along cut surface normal (N)
F_p	Cutting force orthogonal to F_c and F_f (N)
K_{i1}	Specific "cutting" force at the unit area for F_f $(i=c,f,p)$ in ploughing regime (N/μm^2)
K_{i2}	Specific cutting force at the unit area for F_i $(i=c,f,p)$ in shearing regime (N/μm^2)
K_{i3}	Specific cutting force at the unit length for F_i $(i=c,f,p)$ in shearing regime (N/μm)
α_{i1}	Coefficient for ploughing regime $(i=c,f,p)$
α_{i2}	Coefficient for shearing regime $(i=c,f,p)$
K_i	Force per unit of area $(i=c,f,p)$
μ	Friction coefficient

1 Introduction

The increasing development of micro-cutting processes such as micro-milling in recent times has led to a desire to understand and model the mechanisms of chip formation at this scale. Most of the research found in the literature identified a model for micro-cutting directly from micro-milling results. These models usually took into consideration some size effects such as cutting edge radius, tool dynamics and stiffness, ploughing effects, run-out and material heterogeneity.

These main issues in micro-milling are indeed linked to size effects as pointed out by Cheng and Huo [1]. The tools used for micro-milling are clearly different from conventional scale tools, with a greater length compared with diameter and are relatively sharper compared with conventional tools [2]. Such a difference led to considering important influences on cutting forces that are amplified at a micro-scale, such as specific cutting forces [3, 4], burr formation [5] or tool deflection [6]. Other issues, such as vibrations [7–9] or material heterogeneity [10, 11], have been proven to influence cutting forces in micro-milling. The difficulty in identifying parameters for each size effect resulted in them being studied independently but with some limitations.

Bissacco et al. [12] assumed that the cutting edge radius size effect is the most influential parameter on cutting forces and that the rake angle can be considered to be an effective negative rake angle for an uncut chip thickness smaller than the cutting edge radius. They included this effective angle in the cutting coefficient for the Unified Mechanics of a Cutting Model by Armarego [13]. To identify the different coefficients, they performed orthogonal cutting tests with different uncut chip thickness to edge radius ratios and different nominal rake angles. These tests showed that for a ratio lower than 0.5, the cutting forces were no longer influenced by the nominal rake angle. They then verified the model for micro-milling and found good agreement between predicted and measured forces. They also stated that the small end mill run-out had no effect because the tool deflection reduced the imbalance between the cutting forces on the two flutes. Altintas and Jin [14] proposed a model for specific cutting force coefficients including the uncut chip thickness and the cutting edge radius, with five coefficients that were identified by a slip line model of orthogonal cutting and a Johnson-Cook constitutive law. The cutting forces in micro-milling were then obtained by integrating the elementary forces along the cutting edge. The comparison with experimental results needed a Kalman filter to compensate for the distortion resulting from the dynamometer, but showed good agreement. In a similar way, Jing et al. [15] proposed a prediction of cutting forces in micro-milling by identifying specific cutting forces through FEM simulation. These specific cutting forces were identified as a function of the uncut chip thickness and cutting speed. The uncut chip thickness was determined using numerical methods to consider the trochoidal tooth path as well as run-out. In the works of Rodriguez and Labarga [16], a linear model as a function of uncut chip thickness was used to predict cutting forces. The tool run-out, tool deflection and ploughing effect were taking into account to determine the effective uncut chip thickness whatever the location along the cutting edge. A comparison between predicted and experimental cutting forces showed a good degree of agreement, but some vibrations from the process were still unpredicted. Kang et al. [17, 18] as well as Friedrich and Kulkarni [19] took into account elastic recovery in their models. The cutting forces were related to shearing forces during chip formation and sliding forces on the clearance face. These sliding forces were proportional to Young's modulus and the hardness of the machined material. Wang et al. [20] proposed to study chip formation in micro-milling for a half rotation of the tool using FEM simulations. A segmented chip resulted, as was observed during micro-milling experiments.

All these works approximated micro-milling cutting forces with a fairly good agreement, but dynamic effects can hide some chip formation mechanisms at low uncut chip thicknesses notably because of tool stiffness. Decoupling dynamic considerations and chip formation improve the understanding of each contribution. The aim of this work was to model micro-cutting forces based on micro-cutting tests for small uncut chip thicknesses. Thus, dynamic issues were not considered and the assumption of a rigid tool was consistent. This paper presents a model taking into account both ploughing and shearing mechanisms.

2 Experimental set-up

2.1 Elementary cutting set-up

To perform elementary cutting, three methods are often used: disk turning, tube turning or planing. Planing is the closest experimental procedure to performing elementary cutting but is limited by dynamic considerations when reaching high cutting speeds. This limitation can be overridden with turning experimentation where the cutting speed is provided by spindle rotation. Nevertheless, it is necessary to consider some assumptions in elementary cutting. For the tube turning used in this study, two assumptions were verified. The first was the width of cut w (tube thickness) compared with uncut chip thickness h to neglect boundary effects (Eq. (1)).

$$h \gg w \tag{1}$$

The second was that the width of cut has to be limited to minimise the difference between the cutting speed V_{Cinn} at the inner radius R_{inn} and the cutting speed V_{Cout} at the outer radius of the tube R_{out}. The targeted cutting speed V_{Cmed} was

calculated to be in the median radius R_{med}. The expression for the relative error is given by Eq. (2).

$$\frac{\Delta V_C}{V_{Cmed}} = \frac{V_{Cout} - V_{Cinn}}{V_{Cmed}} = \frac{R_{out} - R_{inn}}{R_{med}} = \frac{w}{R_{med}} \quad (2)$$

To adopt these assumptions with the dynamic capabilities of the CNC machine, the tube used in the experiments had an inner radius of 3.024 mm and was 318-μm thick. These dimensions provided a relative error of 10 % for the cutting speed and the thickness of an uncut chip of up to 30 μm. Tube turning also has the advantage of easily performing oblique cutting by moving the cutting edge in a radial direction. Thus, the experiment consisted of an axial displacement of the tube and a machining distance of 0.5 mm. The desired thickness of the uncut chip corresponding to feed per rotation was driven by the axial feed rate. Thus, with measurement occurring over several rotations, the machine stiffness was stabilised after a few rotations and did not influence the experiment. With a cutting speed of 40 m/min, a maximum ratio of about 1:300 between feed rate and cutting speed validated the assumption that the working tool angles during experiment were equal to the nominal tool angles.

The experiments were carried out on a Röders RP600 CNC which performed adequately to ensure minimal errors for the cutting speed, feed rate and position. The chip conveyor was switched off to minimise cutting force signal noise resulting from vibrations.

As shown in Fig. 1, three tools were used as follows: two to obtain the tube dimensions directly before beginning each test from a larger tube to minimise tube run-out and the last to perform the experiments.

Force measurements were carried out using a Kistler Minidyn 9256C2 dynamometer associated with a Kislter amplifier 9017. Data were saved using a National CompactDaq 9174 with NI9215 cards and a dedicated Labview programme. The cutting tools were micro-turning tools IFANGER MTNY 41015-R-TiAlN, which had a cutting edge 1-mm long and a TiAlN coating. The nominal rake angle was investigated using rake angles of 8° and −8°. The cutting edge

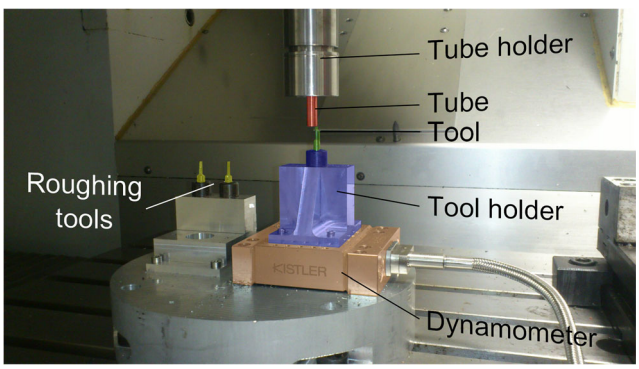

Fig. 1 Experimental set-up for tube turning

radius of each tool was measured using an Alicona Infinite Focus 3D microscope and was close to 1.3 μm. Both the orthogonal and oblique cutting configurations were performed with an inclination angle λ_s of 0° and 30°, respectively.

Because the tool was fixed on the dynamometer, the measured forces were the forces of the material acting directly on the tool on the dynamometer axes, namely F_x, F_y and F_z (Fig. 2). These forces had the shape of a plateau as shown on Fig. 3. The collected data were then treated to compensate for the possible offset and drift of the signal. In the case of the oblique cutting experiments, a geometrical transformation was performed to obtain cutting forces in the desired directions, namely F_c, F_p and F_f (Fig. 2). An automatic detection of cutting force curves was implemented to ensure the same procedure for every experiment. As the entrance and exit of the tool in the material can lead to a peak force, the centre of three quarters of the plateau was used to calculate the average value and standard deviation of the force signal. The experimental device was supported by a digital microscope placed near the cutting zone to ensure the monitoring of tool integrity and to observe, qualitatively, chip formation.

2.2 Workpiece material

The workpiece was 40NiCrMo16 tool steel with heat treatment for hardness up to 54HRC (Fig. 4). Because of the heat treatment, the microstructure showed martensite needles and was considered homogeneous, with a grain thickness of about 100 nm. This material is often used in injection tooling manufacture (injection moulding). All the experiments were carried out on the same tube, and the material behaviour was assumed to be the same all along the tube.

3 Elementary cutting force modelling

The cutting forces model developed in this study consisted of a phenomenological model divided into two terms and predicted the cutting forces F_i (F_c, F_f or F_p) as a function of the uncut chip thickness h, cutting width w and cutting edge radius r_β This depended on cutting constants K_{ij} and α_{ij} The model is given by Eq. (3).

$$F_i = K_{i1}.h.w\left(e^{-\frac{\alpha_{i1}h}{r_\beta}}\right) + (K_{i2}.h + K_{i3}).w.\left(1 - e^{-\frac{\alpha_{i2}h}{r_\beta}}\right) \quad (3)$$

The first term is a linear function proportional to the thickness of the uncut chip and weighted by an exponential function which tends to zero when the thickness of the uncut chip increases. In this way, the cutting force for the uncut chip with the lowest thickness was essentially

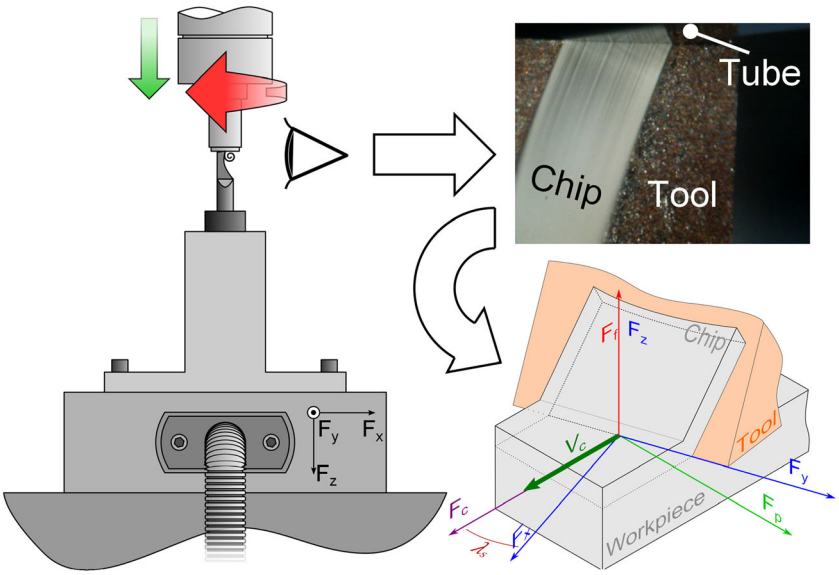

Fig. 2 From turning to oblique cutting

influenced by the first term and represented ploughing regime. Thus, if K_{f1} was greater than K_{c1}, the thrust force was greater than the cutting force for the uncut chip with the lowest thickness because of this first term (Eq. (4)). This term is equal to zero when there is no tool engagement.

$$F_i = K_{i1} \cdot h \cdot w \tag{4}$$

The second term is also a linear function weighted by an exponential function, which tends to one when the thickness of the uncut chip increases to represent shearing regime. For higher values of uncut chip thickness, the cutting forces can be greater than the thrust forces and tend to the well-known model given in Eq. (5).

$$F_i = (K_{i2} \cdot h + K_{i3}) \cdot w \tag{5}$$

Figure 5 shows this decomposition. The exponents are divided by the cutting edge radius to obtain the α coefficients that are unit-less. Moreover, if the cutting edge radius increases, saturation will be observed for the uncut chip with higher thicknesses, increasing the zone of the dominant ploughing regime.

These stages were in good agreement with the dominant ploughing stage and the dominant shearing stage. Moreover, the cutting edge radius appeared exponentially constant: the greater the cutting edge radius, the greater the influence of the ploughing regime on the higher thickness values of the uncut chip. Depending on the two constant values α_1 and α_2, a

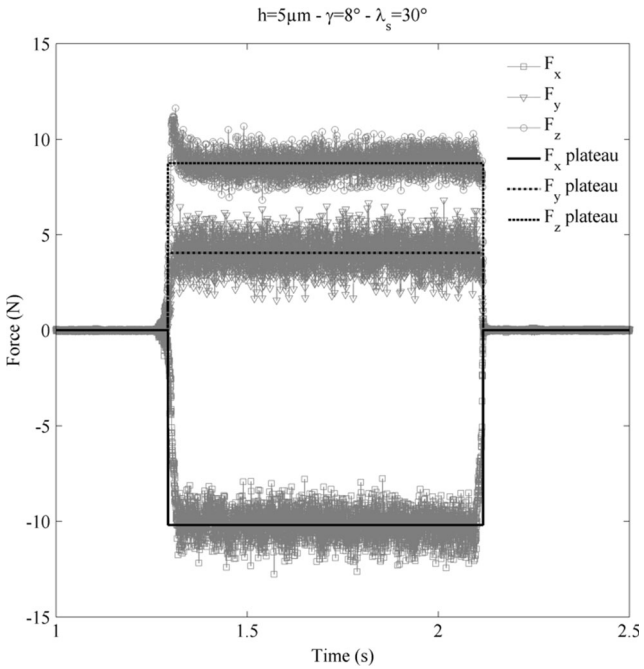

Fig. 3 Experimental cutting forces measured with the dynamometer

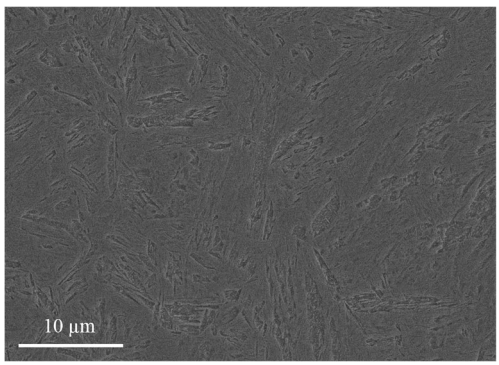

Fig. 4 40NiCrMo16 microstructure

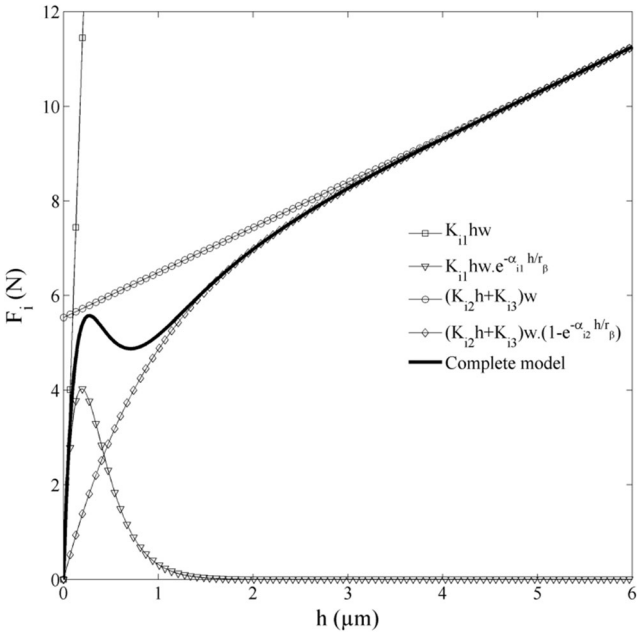

Fig. 5 Force model decomposition as a function of uncut chip thickness h

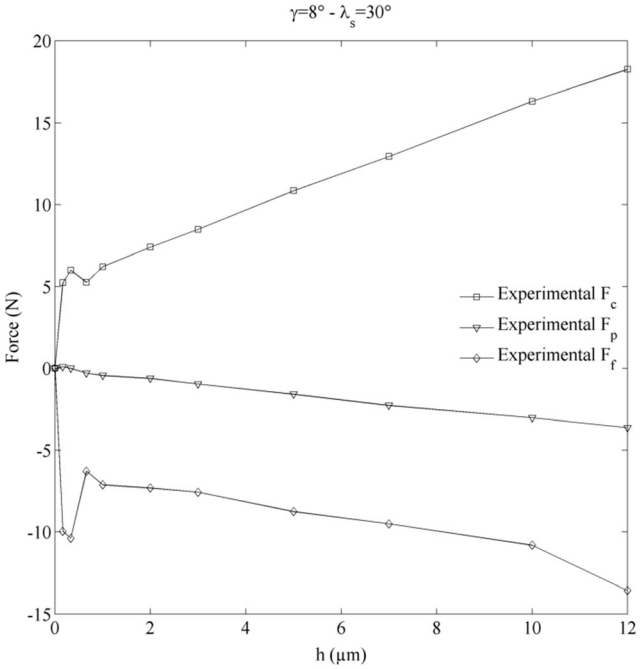

Fig. 6 Experimental results for a rake angle of 8° in oblique cutting ($\lambda_s = 30°$)

transient stage where the two terms were quite equivalent was introduced as shown in Fig. 5.

4 Results and discussion

4.1 Elementary cutting experiment results

Measured cutting forces as a function of the thickness of the uncut chip are presented in Fig. 6. For every cutting configuration, it was noticed that a steep increase up to a local maximum value of forces occurred for thicknesses lower than 1 µm.

This observed jump was the result of the combined action of a change in material composition and local hardening. Indeed, under the action of the ploughing effect at small thicknesses, a layer of the specimen was hardened during the previous path of the tool and the cutting forces increased when the tool attempted to cut into this layer. As the test is cyclical (several rotations in an experiment), the phenomenon compounded with each rotation and was more pronounced when the thickness of the uncut chip was smaller than the hardened layer. Conversely, if the thickness of the uncut chip was greater, the hardened surface from the previous rotation was removed by the formation of the chip, a new hardened surface appeared, and the compounding did not take place.

An SEM observation of the machined surface after the last experiment on the tube presented an affected layer of about 850 nm (Fig. 7). This phenomenon was observed in AISI 1045 by Fleischer et al. [21] for a ratio of the cutting edge radius to the thickness of the uncut chip close to 1. Over a thickness of the uncut chip of 1 µm, cutting forces seem to have a linear behaviour. Reasons for this behaviour are an uncut chip thickness larger than cutting edge radius, erasing cutting edge radius contribution on cutting forces and an uncut chip thickness larger than affected layer thickness, erasing affected layer contribution.

4.2 Parameter identification

Based on these experimental results, model coefficients were identified using MIC2M software. MIC2M [22] is software developed on MATLAB for parameter identification using the Levenberg Marquardt algorithm [23, 24]. The cutting force coefficients in the cutting speed direction F_c, orthogonal to the machined surface F_f and orthogonal to the two previous directions F_p (see Fig. 3), are given, respectively, in Tables 1, 2 and 3. Because F_f and F_p have negative values, absolute

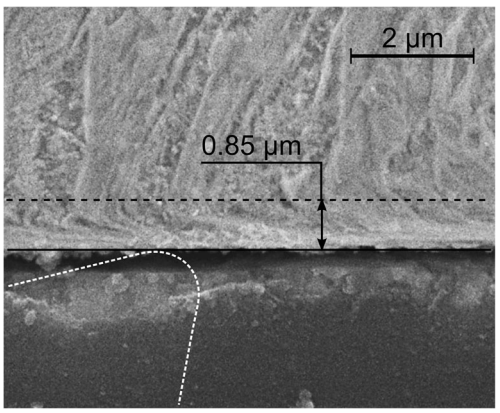

Fig. 7 Microstructure modification under micro-cutting

values were considered for identification to enable comparison with other force components.

As shown in Fig. 8, the identification provides a model that fits experimental results with good agreement. K_{f1} is more than two times greater than K_{c1} in three configurations over four and is explained by the ploughing effect. For the lowest thickness of the uncut chip, the friction on the cutting edge and on the clearance face was more important than the shearing action and led to a higher normal force than the cutting force like a cylinder sliding on a surface. The fact that K_{f3} was higher than K_{c3}, which were the values of the second term of the model when the thickness of the uncut chip decreased, was also an indication of the ploughing effect. A dominant shearing regime was reached when the thickness of the uncut chip increased, leading to K_{f2} being lower than K_{c2}. Nevertheless, it was noticed that for a tool presenting a negative rake angle, coefficients K_f were close to coefficients K_c, which underlined the limited efficiency of shearing localisation compared with a tool with a positive rake angle. The inclination angle λ_s was expected to decrease cutting forces but here, the coefficients increased with the inclination angle. This was caused by a larger contact area between the chip and tool, leading to higher friction forces.

Another observation concerns the coefficients α: for a negative rake angle, the values of these coefficients were greater than those for a positive rake angle and the higher the value, the quicker the exponential factors converged. Therefore, a high value for a coefficient α implied a transient regime for the lower thicknesses of the uncut chip. The second term of the proposed force model influenced the lower thickness of the uncut chip when comparing a negative rake angle with a positive rake angle situation. This is in good agreement with the fact that for the same cutting edge radius, the uncut chip thickness limit was lower for a negative rake angle than for a positive rake angle as stated in other work [12, 18].

Cutting forces per unit of area or specific cutting forces (Eq. 6) are larger than yield strength due to plastic deformation occurring during chip formation and especially in micro-cutting.

$$K_i = \frac{F_i}{h \cdot w} \tag{6}$$

Table 1 F_c cutting force coefficients from identification

γ (°)	8		−8	
λ_s (°)	0	30	0	30
K_{c1} (N/μm^2)	1.817e-1	1.767e-1	9.343e-1	3.682e-1
α_{c1}	6.785	7.452	2.014e1	1.415e1
K_{c2} (N/μm^2)	3.055e-3	3.410e-3	4.725e-3	4.897e-3
K_{c3} (N/μm)	1.738e-2	1.684e-2	2.211e-2	2.437e-2
α_{c2}	1.804	2.299	3.029	3.725

Table 2 F_f cutting force coefficients from identification

γ (°)	8		−8	
λ_s (°)	0	30	0	30
K_{f1} (N/μm^2)	3.964e-1	3.931e-1	2.080	2.127e-1
α_{f1}	6.929	7.405	2.035e1	8.880
K_{f2} (N/μm^2)	1.369e-3	1.786e-3	4.468e-3	4.835e-3
K_{f3} (N/μm)	2.045e-2	1.860e-2	2.266e-2	2.471e-2
α_{f2}	1.747	3.490	5.451	3.508e1

In this model, specific cutting force K_c tends to K_{c1} when uncut chip thickness decreases leading to the ploughing regime and tends to K_{c2} when uncut chip thickness increases leading to the shearing regime. K_c limits in ploughing regime are, respectively, over 170 GPa for a positive rake angle and over 360 GPa for a negative rake angle. These limits decrease, respectively, to 3 and 4.7 GPa in shearing regime. These limits exceed largely yield strength and specific cutting force in conventional cutting which is about 2 GPa. The high limit for ploughing regime is also due to cutting edge radius leading to a larger contact area than $h{\cdot}w$. This discussion is also available for K_f.

An interesting comparison between coefficients K_c and K_f provides information about friction. Except for oblique cutting with a negative rake angle, the ratio K_{c1}/K_{f1} is close to 0.45. This value can be considered as the friction coefficient when no chip formation occurred, in other words, it was close to the friction coefficient of a tool sliding on the material. The ratio K_{c2}/K_{f2} depended largely on the rake angle: for a rake angle of 8° the ratio was close to 2 (1.9 and 2.2) whereas for a rake angle of −8° the ratio equalled 1. Nevertheless, this coefficient was related to the friction coefficient between the chip and rake face. Based on Merchant modelling [25], this friction coefficient can be expressed as Eq. (7) in orthogonal cutting.

$$\mu = \tan\left(\gamma + \arctan\frac{F_f}{F_c}\right) \tag{7}$$

Table 3 F_p cutting force coefficients from identification

γ (°)	8		−8	
λ_s (°)	0	30	0	30
K_{p1} (N/μm^2)	In orthogonal cutting $F_p = 0$ N	−1.155e-2	In orthogonal cutting $F_p = 0$ N	−2.730e-2
α_{p1}		8.154		1.567e1
K_{p2} (N/μm^2)		9.237e-4		1.268e-3
K_{p3} (N/μm)		3.596e-4		9.146e-4
α_{p2}		8.156		2.127e-1

When the thickness of the uncut chip increases, in orthogonal cutting, the F_f/F_c ratio tends to K_{f2}/K_{c2}. Thus, Eq. (7) is close to Eq. (8).

$$\mu = \tan\left(\gamma + \arctan\frac{K_{f2}}{K_{c2}}\right) \tag{8}$$

Based on the results obtained in orthogonal cutting, the friction coefficient equals to 0.7. This coefficient was higher than the ratio K_{c1}/K_{f1} and proved that sliding was more difficult for the chip on a rake face, and that sticking phenomena occurred.

Ratio K_{c3}/K_{f3} was less influenced by the rake angle and was close to 0.9 for the positive rake angle and 0.95 for the negative rake angle. Because the K_{c3} and K_{f3} coefficients provided the second-term values of the model when the thickness of the uncut chip tended to zero, no influence from the rake angle was expected. Because F_p forces were generally smaller than the other two components, the ploughing regime was more difficult to identify for F_p forces.

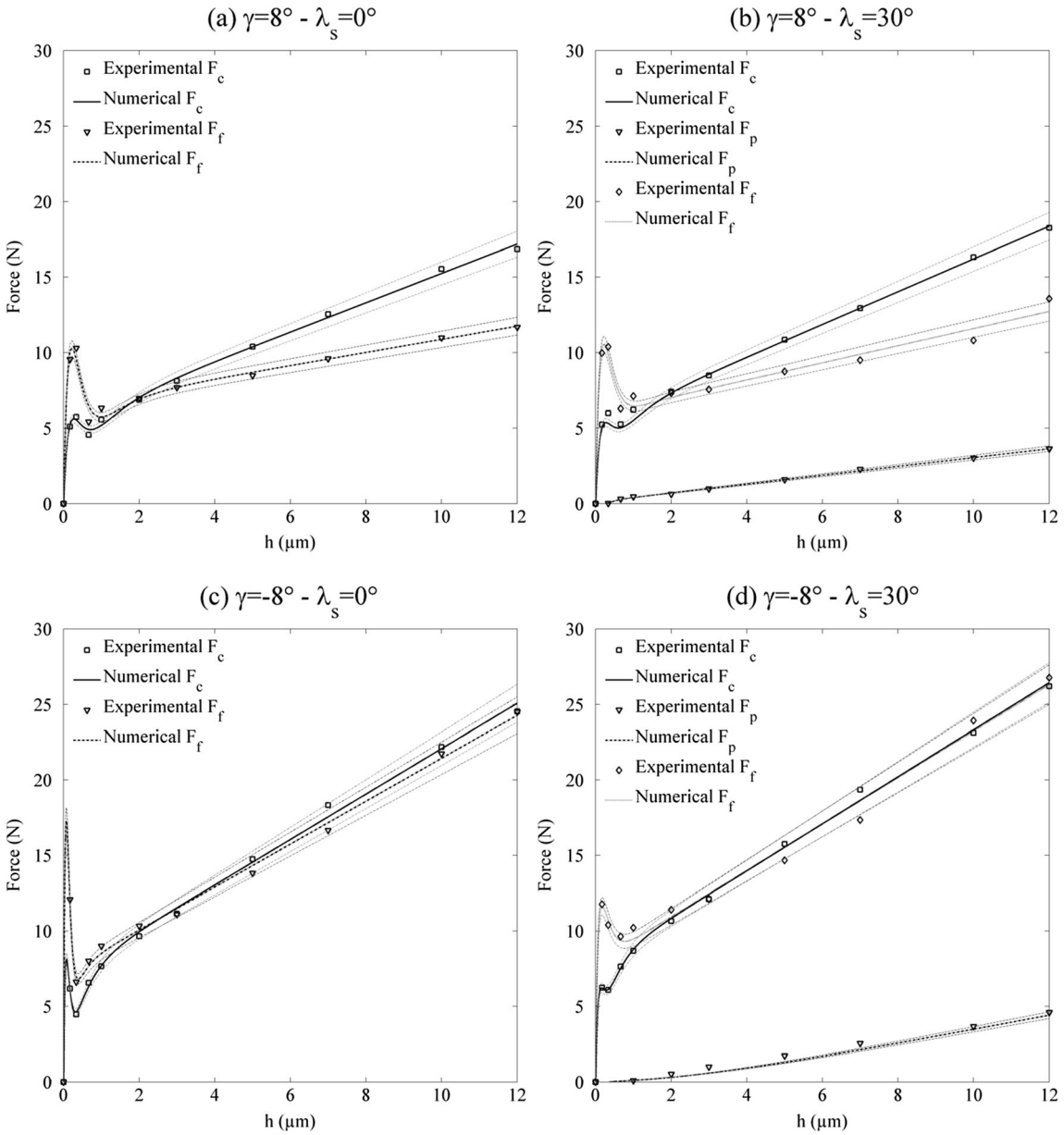

Fig. 8 Comparison between results obtained from the experiments and model (±5 %). **a** Rake angle $\gamma = 8°$, inclination angle $\lambda_s = 0°$. **b** Rake angle $\gamma = 8°$, inclination angle $\lambda_s = 30°$. **c** Rake angle $\gamma = -8°$, inclination angle $\lambda_s = 0°$. **d** Rake angle $\gamma = -8°$, inclination angle $\lambda_s = 30°$

5 Conclusions

This study presents a phenomenological modelling of cutting forces that can be used to predict micro-cutting forces. The model takes into account the ploughing regime for low thicknesses of the uncut chip. For higher thicknesses of the uncut chip, the model tends to the well-known linear model. Based on elementary cutting experiments, the parameters of the model were identified. Because the tools used can be considered as rigid bodies, these experiments avoid the dynamic considerations inherent in micro-milling. A peak or jump in cutting forces was observed in the experiments and was identified as the dominant ploughing regime in a hardened layer. The identified parameters of the proposed model presented satisfactory agreement with the experimental results. The influence of the cutting edge radius, rake angle and friction was clearly observed.

An implementation of this model in micro-milling force prediction will provide essential information on the dynamic issues occurring in micro-milling. The numerical approach to elementary cutting using a meshless method, and a quick stop device will also assist the comparison of dominant compositions during chip formation and improve the modelling with thermomechanical considerations.

Acknowledgments The authors wish to acknowledge the Ministère de l'Education Nationale, de l'Enseignement Supérieur et de la Recherche (MENESR) for their financial support. This work was developed in the context of the Manufacturing'21 research group gathering 18 french laboratories in the field of advanced manufacturing. The authors also thank Gaël Le Coz from USINOV platform for his technical support.

References

1. Cheng K, Huo D (2013) Micro-cutting fundamentals and applications. Wiley
2. Dornfeld D, Min S, Takeuchi Y (2006) Recent advances in mechanical micromachining. CIRP Ann Manuf Technol 55:745–768. doi:10.1016/j.cirp.2006.10.006
3. Aramcharoen A, Mativenga PT (2009) Size effect and tool geometry in micromilling of tool steel. Precis Eng 33:402–407. doi:10.1016/j.precisioneng.2008.11.002
4. Sawangsri W, Cheng K (2016) An innovative approach to cutting force modelling in diamond turning and its correlation analysis with tool wear. Proc Inst Mech Eng Part B J Eng Manuf 230:405–415
5. Mian A, Driver N, Mativenga PT (2011) Identification of factors that dominate size effect in micro-machining. Int J Mach Tools Manuf 51:383–394. doi:10.1016/j.ijmachtools.2011.01.004
6. Biermann D, Kahnis P (2010) Analysis and simulation of size effects in micromilling. Prod Eng 4:25–34
7. Afazov SM, Ratchev SM, Segal J, Popov AA (2012) Chatter modelling in micro-milling by considering process nonlinearities. Int J Mach Tools Manuf 56:28–38. doi:10.1016/j.ijmachtools.2011.12.010
8. Afazov SM, Zdebski D, Ratchev SM et al (2013) Effects of micro-milling conditions on the cutting forces and process stability. J Mater Process Technol 213:671–684. doi:10.1016/j.jmatprotec.2012.12.001
9. Malekian M, Park SS, Jun MBG (2009) Modeling of dynamic micro-milling cutting forces. Int J Mach Tools Manuf 49:586–598
10. Vogler MP, DeVor RE, Kapoor SG (2003) Microstructure-level force prediction model for micro-milling of multi-phase materials. J Manuf Sci Eng 125:202–209
11. Mian AJ, Driver N, Mativenga PT (2010) A comparative study of material phase effects on micro-machinability of multiphase materials. Int J Adv Manuf Technol 50:163–174
12. Bissacco G, Hansen HN, Slunsky J (2008) Modelling the cutting edge radius size effect for force prediction in micro milling. CIRP Ann Manuf Technol 57:113–116. doi:10.1016/j.cirp.2008.03.085
13. Armarego EJA (1998) A generic mechanics of cutting approach to predictive technological performance modeling of the wide spectrum of machining operations. Mach Sci Technol 2:191–211
14. Altintas Y, Jin X (2011) Mechanics of micro-milling with round edge tools. CIRP Ann Manuf Technol 60:77–80
15. Jing X, Li H, Wang J, Tian Y (2014) Modelling the cutting forces in micro-end-milling using a hybrid approach. Int J Adv Manuf Technol 73:1647–1656. doi:10.1007/s00170-014-5953-x
16. Rodríguez P, Labarga JE (2015) Tool deflection model for micromilling processes. Int J Adv Manuf Technol 76:199–207. doi:10.1007/s00170-014-5890-8
17. Kang IS, Kim JS, Kim JH et al (2007) A mechanistic model of cutting force in the micro end milling process. J Mater Process Technol 187–188:250–255. doi:10.1016/j.jmatprotec.2006.11.155
18. Kang IS, Kim JS, Seo YW (2008) Cutting force model considering tool edge geometry for micro end milling process. J Mech Sci Technol 22:293–299. doi:10.1007/s12206-007-1110-x
19. Friedrich CR, Kulkarni VP (2004) Effect of workpiece springback on micromilling forces. Microsyst Technol 10:472–477. doi:10.1007/s00542-004-0375-6
20. Wang J, Gong Y, Abba G et al (2009) Chip formation analysis in micromilling operation. Int J Adv Manuf Technol 45:430–447
21. Fleischer J, Schulze V, Kotschenreuther J (2009) Extension of cutting force formulae for microcutting. CIRP J Manuf Sci Technol 2:75–80
22. Richard F (1999) Identification du comportement et évaluation de la fiabilité des composites stratifiés. UFC
23. Levenberg K (1944) A method for the solution of certain non-linear problems in least squares. Q Appl Math 2:164–168
24. Marquardt DW (1963) An algorithm for least-squares estimation of nonlinear parameters. J Soc Ind Appl Math 11:431–441
25. Merchant ME (1945) Mechanics of the metal cutting process. I. Orthogonal cutting and a type 2 chip. J Appl Phys 16(5):267–275